Preprints (www.preprints.org) | NOT PEER-REVIEWED | Posted: 29 December 2016 doi:10.20944/preprints201612.0145.v1

Article

Structural Insights into *Thermotoga maritima* FtsH Periplasmic Domain on Substrate Recognition

Jun Yop An[1,2], Humayun Sharif[1,2,a,b], Gil Bu Kang[1,c], Kyung Jin Park[1,2], Jung-Gyu Lee[1,2], Sukyeong Lee[3], Mi Sun Jin[1], Ji-Joon Song[4], Jimin Wang[2,5,*], Soo Hyun Eom[1,2,*]

[1] School of Life Sciences, Gwangju Institute of Science and Technology, Gwangju 61005, Republic of Korea
[2] Steitz Center for Structural Biology, Gwangju Institute of Science and Technology, Gwangju 61005, Republic of Korea
[3] Verna and Marrs McLean Department of Biochemistry and Molecular Biology, Baylor College of Medicine, Houston, Texas 77030, USA
[4] Department of Biological Sciences, KI for the BioCentury, Cancer Metastasis Control Center, KAIST, Daejeon, 34141, Republic of Korea
[5] Department of Molecular Biophysics & Biochemistry, Yale University, New Haven, CT 06520, USA
Current addresses:
[a] Department of Cancer Biology, Dana-Farber Cancer Institute, 450 Brookline Avenue, Boston, MA 02215, USA
[b] Department of Biological Chemistry and Molecular Pharmacology, Harvard Medical School, Boston, MA 02115, USA
[c] Research & Development Center, GreenCross Inc., Ihyeon-ro 30 beon-gil, Giheung-gu, Yongin-si, Gyeonggi-do, 16924, Republic of Korea
[*]Author to whom correspondence should be addressed:
E-mail: eom@gist.ac.kr (Phone: +82-62-715-2519; Fax: +82-62-715-2521) or jimin.wang@yale.edu

Abstract: Prompt removal of misfolded membrane proteins and misassembled membrane protein complexes is essential for membrane homeostasis. However, the elimination of these toxic proteins from the hydrophobic membrane environment has high energetic barriers. Transmembrane FtsH is the only known ATP-dependent protease responsible for this task, unlike other well-studied soluble ATP-dependent proteases. The mechanisms by which FtsH recognizes, unfolds, translocates, and proteolyzes its substrates remain unclear. Here, we report the crystal structures of the *Thermotoga maritima* FtsH periplasmic domain (PD) in an associative trimeric state at a 1.5-1.95 Å resolution. We also describe the pH-dependent oligomerization states of the isolated PD using dynamic light scattering. These observations help us understand how FtsH recognizes membrane-anchored misfolded proteins.

Keywords: ATP-dependent proteolysis; Non-native membrane proteins; Periplasmic domain; Crystal structure; Photosystem II.

1. Introduction

If denatured proteins were allowed to accumulate in membranes, they would rapidly compromise cellular functions because the available membrane space is limited. Denatured proteins may result from oxidative damage, misfolding, missing prosthetic groups, or imbalanced synthesis of oligomeric components [1]. They may also exist as intermediates in degradation pathways. Since the denatured states of membrane proteins are constrained by the lipid environment, the enzymes that identify and help degrade them confront a difficult task compared to proteases responsible for the turnover of soluble proteins. Here, we uncover a potential mechanism by which membrane enzymes identify and degrade denatured membrane proteins.

FtsH and its homologs are the only ATP-dependent proteases essential for membrane protein quality control in bacteria and in the organelles of bacterial origin, such as the mitochondria in yeast

Preprints (www.preprints.org) | NOT PEER-REVIEWED | Posted: 29 December 2016 doi:10.20944/preprints201612.0145.v1

and mammals and chloroplasts in plants [1]. The FtsH proteases display ATPase and peptidase activities within a single-polypeptide. They are highly conserved, sharing at least 40% sequence identity among all species homologs examined thus far [1-2]. The ATPase domain contains Walker A and B motifs, and belongs to the ATPase-associated diverse cellular activities (AAA+) superfamily [3]. The peptidase domain belongs to the M41 Zn-metallopeptidase family [4]. Most bacteria have a single *FtsH* gene, while yeast and humans have three. However, plants have as many as 12 orthologs, and this expansion is likely related to the maintenance of photosystems. FtsH is a component of the FtsH/DegP (or HtrA) protease network, which is responsible for the repair of proteins that compose photosystem II in plants and cyanobacteria, where D1 and D2 domains are often subjected to oxygenic damage under continuous light or UVB radiation conditions [5]. Soluble DegP makes specific cuts in the soluble loops of the damaged D1 and D2 domains, releasing individual transmembrane (TM) helices so that FtsH can recognize and degrade them. However, FtsH alone is necessary and sufficient for this repair process based on gene inactivation studies in cyanobacteria [6], whereas DegP is not.

In addition, mitochondria also have two types of FtsH proteases in their inner (cytoplasmic) membrane, which are classified according to the location of the catalytic domain either in the *i*ntermembrane or *m*atrix space (*i*-AAA or *m*-AAA, respectively). Bacterial FtsHs and nearly all eukaryotic FtsHs have two conserved TM helices, TM1 and TM2. These helices flank a soluble periplasmic domain (PD) shown schematically in Figure 1A [7].

FtsH forms a homohexamer and interacts with both membrane protein substrates and non-membrane substrates [2,7-10]. In *Escherichia coli*, FtsH substrates in the inner membrane have been identified [11-13]. *E. coli* FtsH is responsible for the rapid degradation of the unassembled components of SecY inside the membrane [2,14], ensuring that the SecY translocase is always stoichiometrically assembled with the correct subunits for co-translational insertion and folding of membrane proteins. If unassembled membrane proteins are not promptly removed, they may become toxic to the cell by directly interfering with other membrane proteins and by otherwise taking up valuable space in the highly concentrated environment of the plasma membrane. Thus, rapid removal of unassembled or misfolded proteins is essential for membrane homeostasis. This is a surprisingly complex task because 20-30% of all genomic open reading frames encode proteins possessing at least one TM helix [15]. Additionally, FtsH has many other diverse functions unrelated to its quality control of the membrane proteins. As evidence of this, FtsH was discovered repeatedly in a variety of biological contexts and assigned different names, such as *mrs*C, *tol*Z, and *hlf*B [2]. This explains why past studies specifically focused on understanding its proteolytic activities upon soluble protein substrates. However, it is now recognized that pertinent substrates actually reside within the plasma membrane, and current research is focusing on the mechanisms of substrate recognition and processing. Unlike soluble ATP-dependent proteases that thread substrates into an ATPase-peptidase chamber through either the free N- or C-terminus [16], FtsH degrade protein substrates that lack free ends by initiating proteolysis from internal motifs of nonnative substrates [17]. Here, we report high-resolution crystal structures of the FtsH-PD from *Thermotoga maritima* (*tm*PD) at pH 6.0 and pH 5.5 to a resolution of 1.95 and 1.50-Å, respectively. We also examined pH-dependent oligomerization states of isolated PD using dynamic light scattering. This study provides evidence for multiple oligomeric states of *tm*PD, which has important implications for substrate recognition.

Preprints (www.preprints.org) | NOT PEER-REVIEWED | Posted: 29 December 2016 doi:10.20944/preprints201612.0145.v1

2. Results and discussion

2.1. Crystal structure of tmPD

The PD and cytoplasmic domains of FtsH encounter different pH environments separated by the cell membrane. The rapid growth of many bacteria produces cytoplasmic lactic acid as a byproduct of glycolysis. To maintain cytoplasmic pH (pH 7.2 to 7.8), protons are pumped out of the cell, acidifying the periplasm and extracellular environments [18]. Membrane proteins, such as FtsH, find their PD and cytoplasmic domains localized in different pH environments separated by the membrane with the PD in a more acidic space. We found that *tm*PD underwent a pH-dependent oligomerization and explored this behavior under slightly acidic conditions, which favors *tm*PD hexamerization. Indeed, under conditions in which hexamer formation is favored, *tm*PD readily crystallized. We therefore determined the crystal structure of SeMet-incorporated *tm*PD at pH 6.0 to a resolution of 1.95 Å (PDB code 4Q0F) using the SeMet-MAD phasing method. Subsequently, we obtained a second structure of *tm*PD at pH 5.5. In this case, the protein crystallized in a nearly identical form, but this condition yielded even better diffraction to a 1.50-Å resolution (Table 1, PDB code 4M8A).

Table 1. Data collection and refinement statistics

Data Collection	**FtsH-PD Native**	**FtsH-PD SeMet Derivative**			
		Inflection	**Peak**	**H-Remote**	**L-Remote**
X-ray source			PAL-4A		
Wavelength (Å)	1.0000	0.97924	0.97901	0.97134	0.98696
Space group			$P2_12_12$		
Cell dimensions (Å)	a = 41.8 b = 65.8 c = 71.8		a = 42.0 b = 66.0 c = 71.9		
Resolution (Å)[a]	50 – 1.50 (1.53-1.50)		50 – 1.95 (1.98-1.95)		
Total reflections	369559	202114	200241	202640	202100
Unique reflections	31852	14862	14851	14798	14875
Completeness (%)	99.6 (99.9)	99.8 (100)	99.8 (100)	99.8 (100)	99.7 (100)
R_{merge}[b]	0.040 (0.253)	0.069 (0.264)	0.073 (0.262)	0.069 (0.287)	0.063 (0.248)
Mean <I/σ (I)>	27.9(13.0)	19.9(16.3)	19.9(17.2)	19.4(15.2)	20.5(17.6)
Refinement Statistics					
Resolution (Å)	31.7 - 1.50		36.3 – 1.95		
R_{work}[c]	0.161		0.209		

Preprints (www.preprints.org) | NOT PEER-REVIEWED | Posted: 29 December 2016 doi:10.20944/preprints201612.0145.v1

R_{free}[d]	0.202	0.254
Rms deviations		
Bond lengths (Å)	0.007	0.003
Bond angles (°)	1.027	0.639
Ramachandran plot		
Favored (%)	98.6	96.9
Allowed (%)	1.4	3.1
Number of water molecules	233	87
PDB accession code	4M8A	4Q0F

[a] Values in parentheses are for the highest resolution shell.

[b] $R_{merge} = \sum_{hkl} \sum_i |I_i(hkl) - \langle I(hkl) \rangle| / \sum_{hkl} \sum_i I_i(hkl)$, where $I_i(hkl)$ is the intensity of the ith observation of reflection hkl and $\langle I(hkl) \rangle$ is the average intensity of reflection hkl.

[c] $R_{work} = \Sigma \big| |F_o| - |F_c| \big| / \Sigma |F_o|$, where F_o and F_c are the observed and calculated structure factors, respectively.

[d] R_{free} was calculated using 5% of the randomly selected unique reflections that were omitted from structure refinement

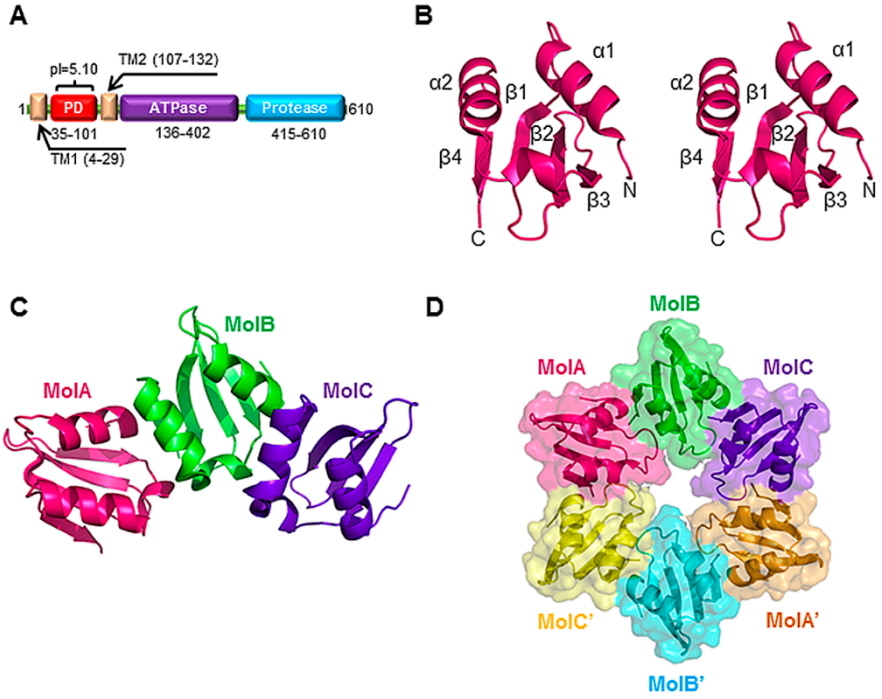

Figure 1. Domain organization and structure of *tm*PD. (A) Domain organization of *tm*PD, comprising TM1, PD, TM2, ATPase, and the protease domain. The isoelectric point of PD was calculated with Protein Calculator v3.4 (http://protcalc.sourceforge.net). (B) Stereoview of ribbon diagrams of monomeric structure of *tm*PD. (C) Trimeric structure of *tm*PD in an asymmetric unit. (D) Computationally assembled hexamer by two-fold symmetry operation applied to the trimeric structure.

Preprints (www.preprints.org) | NOT PEER-REVIEWED | Posted: 29 December 2016 doi:10.20944/preprints201612.0145.v1

The overall structure of *tm*PD has an αββββαβ fold with four β-strands on its concave face (β-face) and two α-helices on its convex face (α-face) (Figure 1B). In addition, a short 3_{10} helix is located in between β3 and α2. In the crystals, *tm*PD exists as a trimeric half hexamer in which three subunits are in contact with each other and are related by an approximate 6-fold symmetry (Figure 1C). Upon application of a 2-fold symmetry operation, the trimer generates a full hexamer with a solvent-accessible axial pore of about 10 Å in diameter (Figure 1D). A structural similarity search shows that *tm*PD has a fold similar to other domains involved in protein-protein or protein-ligand interactions (Table S1).

2.2 Asymmetric charge distribution in the tmPD hexamer

The *tm*PD (residues 35-101) has a calculated isoelectric point of 5.1 (Figure 1A). It possesses 12 acidic residues evenly distributed throughout the subunit surface and 10 unevenly distributed basic residues in addition to its amino terminus. Basic residues are absent at the central pore where only acidic residues are present (Figure 2A). To investigate whether this uneven charge distribution across the PD hexamer is important for pH-dependent oligomerization, we replaced both D59 and D83 with asparagine residues near the pore (Figure 2B). This caused a substantial shift in the oligomerization pH profile in the mutant compared to that in the wild type PD (Figure 2C). The slopes of the pH-dependent transitions are likely a function of the cooperativity among subunits. This provides a structural basis for the asymmetric actions of the PD and TM domains during the extraction of denatured membrane proteins. A calculation of the isoelectric points of individual domains of other FtsH proteases shows that the PDs are generally more acidic than the corresponding cytoplasmic domains among all species examined (Table S2). This observation is consistent with the positive-inside rule [19], and suggests a common pH-dependent regulation of this enzyme.

Preprints (www.preprints.org) | NOT PEER-REVIEWED | Posted: 29 December 2016 doi:10.20944/preprints201612.0145.v1

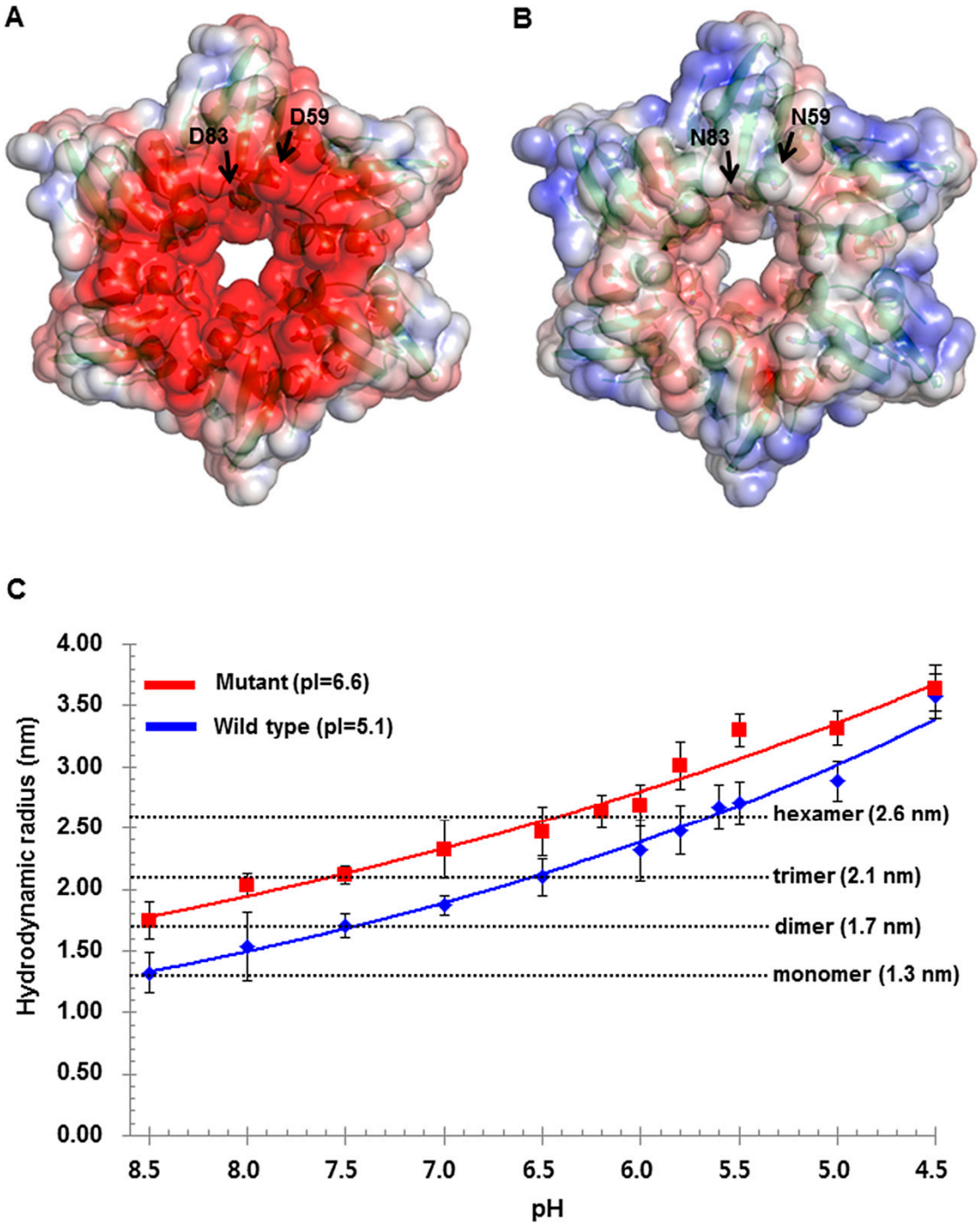

Figure 2. Surface charge distribution and pH-dependent multimerization of wild-type and mutant *tm*PD. (A) Surface charge distribution for hexameric *tm*PD. Highly negative charges developed at the pore region of wild-type *tm*PD. Solvent-accessible electrostatic surface potential was calculated with the PDB2PQR server (http://nbcr-222.ucsd.edu/pdb2pqr_2.1.1/) and contoured at ± 6 kT/e. (B) Surface charge distribution of mutant *tm*PD (D59N/D83N). Negative charges diminished at the pore region upon mutation of D59N and D83N. (C) pH-dependent multimer formation of *tm*PD. A pH-dependent hydrodynamic radius of the *tm*PD oligomers was determined using the dynamic light scattering method for the wild-type and D59N/D83N mutant *tm*PD (Avidnano W130i and the *i*-Size™ software). Theoretical R_H values for the monomeric, dimeric, trimeric, and hexameric *tm*PD were calculated using the program Hydropro [20]. Protein Calculator v3.4 (http://protcalc.sourceforge.net) was used to calculate pI values.

Preprints (www.preprints.org) | NOT PEER-REVIEWED | Posted: 29 December 2016 doi:10.20944/preprints201612.0145.v1

2.3 Structural comparison of tmPD and ecPD

The crystal structure of *tm*PD was determined as a trimer using purified monomeric *tm*PD (at 1.5-1.95 Å resolution). We verified various oligomeric states over a wide range of pH values. In contrast, *E. coli* FtsH PD (*ec*PD) was purified as a monomer and its structure was determined as a monomer and hexamer by NMR and X-ray crystallography (at 2.55 Å resolution), respectively [21]. The structures of *tm*PD and *ec*PD superimpose well, yielding the root-mean-squire deviation (RMSD) of 1.37 Å and 1.68 Å for the monomer (60 Cα atoms) and the hexamer (329 Cα atoms), respectively. Hydrophobic residues at the subunit interface of the two structures are also highly conserved (Figure 3A). However, the charge distribution at the pore region between the two structures is quite different. Non-polar residues are observed at the pore region for *ec*PD, while *tm*PD has negatively charged residues near the pore region (*ec*PD; G53, P75, D79: *tm*PD; D59, D83, D88). This is consistent with the labile hexamer formation in the *tm*PD (Figure 3B). Collectively, these data suggest that *tm*PD likely associates and dissociates in hexameric full-length FtsH, while the other domains help maintain a stable hexameric form.

Preprints (www.preprints.org) | NOT PEER-REVIEWED | Posted: 29 December 2016 doi:10.20944/preprints201612.0145.v1

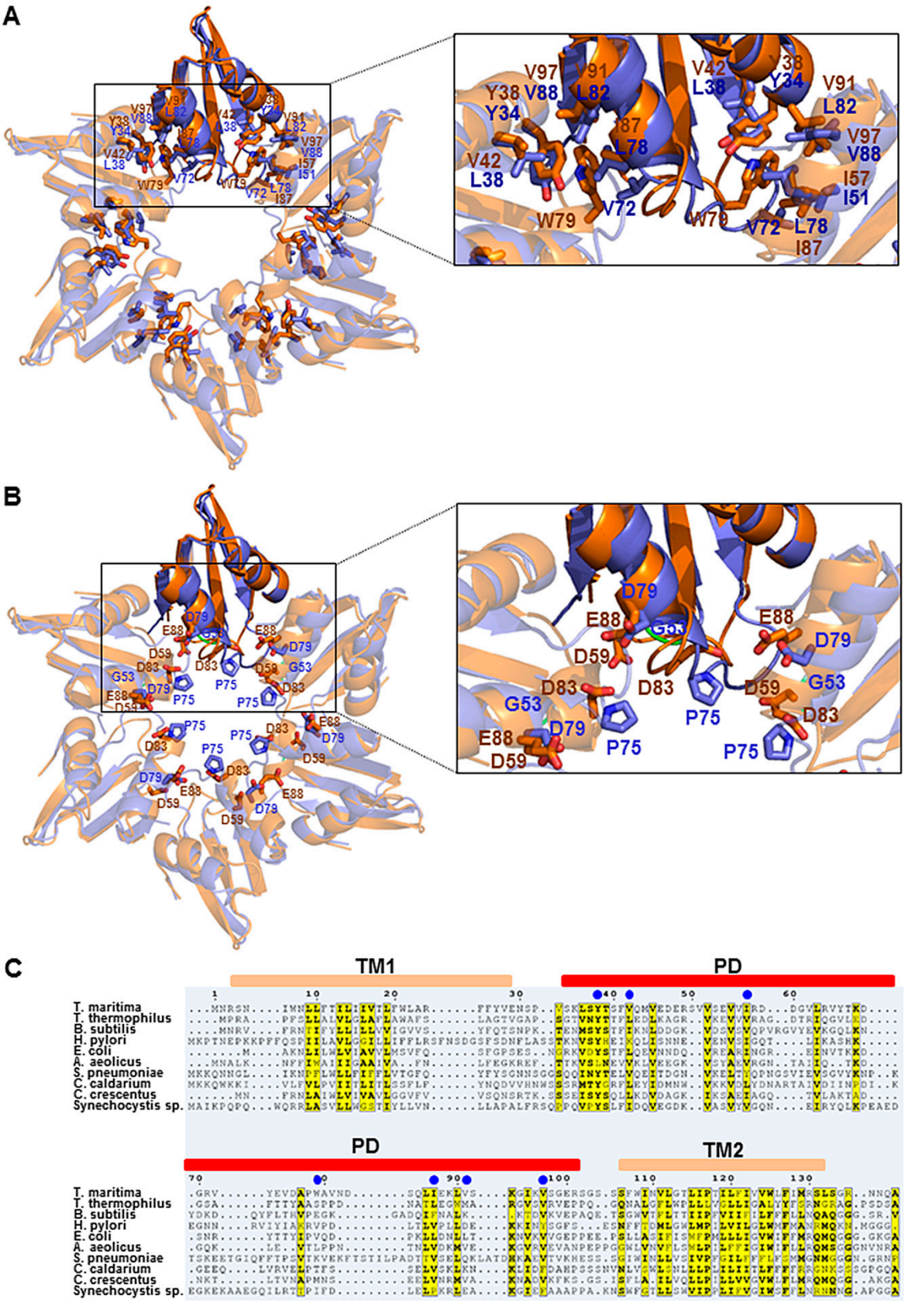

Figure 3. Comparison of residues at the interface of *tm*PD versus *ec*PD. (A) Hydrophobic residues at the interface. *tm*PD is shown in orange and *ec*PD in blue. (B) Residues at the pore region. Gly53 of *ec*PD is colored green (C) Multiple sequence alignment of PDs. Sequence alignment was performed

Preprints (www.preprints.org) | NOT PEER-REVIEWED | Posted: 29 December 2016 doi:10.20944/preprints201612.0145.v1

with the program ClustalX1.8 [22] and visually represented using ESPript3.0 (http://espript.ibcp.fr/ESPript/cgi-bin/ESPript.cgi) [23]. Hydrophobic residues at the subunit interface of *tm*PD are marked with blue dots (Tyr38, Val42, Ile57, Ile87, W79, Val91, and Val97).

2.4 Significance of dynamics of tmPD multimerization

At the subunit interface of the hexamer, backbone hydrogen bonds and charged residues define the specificity of hexamerization. This is because the two complementary hydrophobic surfaces are relatively flat, permitting alternative subunit-subunit interactions. These hydrophobic surfaces are composed of I57, I87, V91, and V97 in one subunit and Y38, V42, and W79 in the other. The presence of these types of hydrophobic surfaces is generally conserved among AAA proteases (Figure 3C). They might be exposed in the monomeric form, possibly providing a binding site for unfolded proteins (Figure 4). This would be consistent with the previous observation that deletion of the intermembrane space domain corresponding to PD, along with two TMs, disables the enzyme's ability to proteolyze membrane proteins [24, 25].

The observed pH-dependent oligomerization of *tm*PDs implies that the periplasmic pH can modulate the equilibrium between the two functional states, and, therefore, influence FtsH activity. When the pH at the periplasm matches the pI of the PD of FtsH, the transition between the two states has a reduced energetic barrier. It consumes less free energy so that the full amount of energy stored in ATP can be used for the extraction of denatured membrane proteins. Considering that the monomer-hexamer transition of the isolated PD occurs within 2.5 pH units or about 320-fold change in proton concentration (Figure 3), the pH can shift the monomer-hexamer equilibrium by about 3.4 kcal/mol [$\Delta\Delta G$=-RT*ln* (proton concentration ratio)]. However, the actual energy difference between the two states might be much smaller because the exposed hydrophobic surfaces of the non-associative PD domain may induce structural changes in the membrane, allowing PD to interact with it before binding non-native membrane proteins. These surfaces are buried in the associative hexameric PD state and exposed in the monomeric state. If the hexameric PD indeed represents a form after substrate capture, FtsH would be more active when periplasm is acidic near 5.5 to 6.0 than when it is near 7.2 to 7.8. This pH-dependent behavior of *tm*FtsH may also highlight a species-specific functional difference between *tm*FtsH and *ec*FtsH and perhaps among other. Cumulatively, this study describes the dynamic nature of *tm*PD oligomerization, which might be relevant for the recognition of some substrates (Figure 4).

One class of TM proteins may contain folded periplasmic domains, which could be partially unfolded and thus become substrates for FtsH after partial degradation by soluble proteases such as DegP. The partially unfolded domains of the TM proteins could exhibit high affinity for partially dissociative trimeric or monomeric PD of FtsH, which resembles the tentacles of an octopus, waiting for prey (Figure 4). Once a substrate is bound, the equilibrium would be shifted in favor of PD hexamerization (Figure 4). PD hexamer could then segregate a single TM helix of the substrate and enclose it inside the central channels of the hexameric PD, the TM domain, and the peptidase compartment of FtsH for ATP-dependent proteolysis. The nature of the TM domain of hexameric FtsH remains under active investigations using both experimental and computational approaches. A preliminary EM analysis suggests that the TM domain of hexameric of *m*-AAA protease may indeed be capable of enclosing single TM helix [26]. Although it requires additional investigation, this mechanism would be an attractive model for repairing and recycling photo-damaged photosystem II in plant leave cells when photosynthesis is highly active during daytime. Photosystem II splits $2H_2O$ molecules into O_2 plus 4 protons and 4 electrons upon absorption of four photons, and protons are pumped to the periplasmic side [27]. When photosystem II is shut off at nighttime, no proton is generated such that periplamsic space is much less acidic and FtsH needs not be very active.

Preprints (www.preprints.org) | NOT PEER-REVIEWED | Posted: 29 December 2016 doi:10.20944/preprints201612.0145.v1

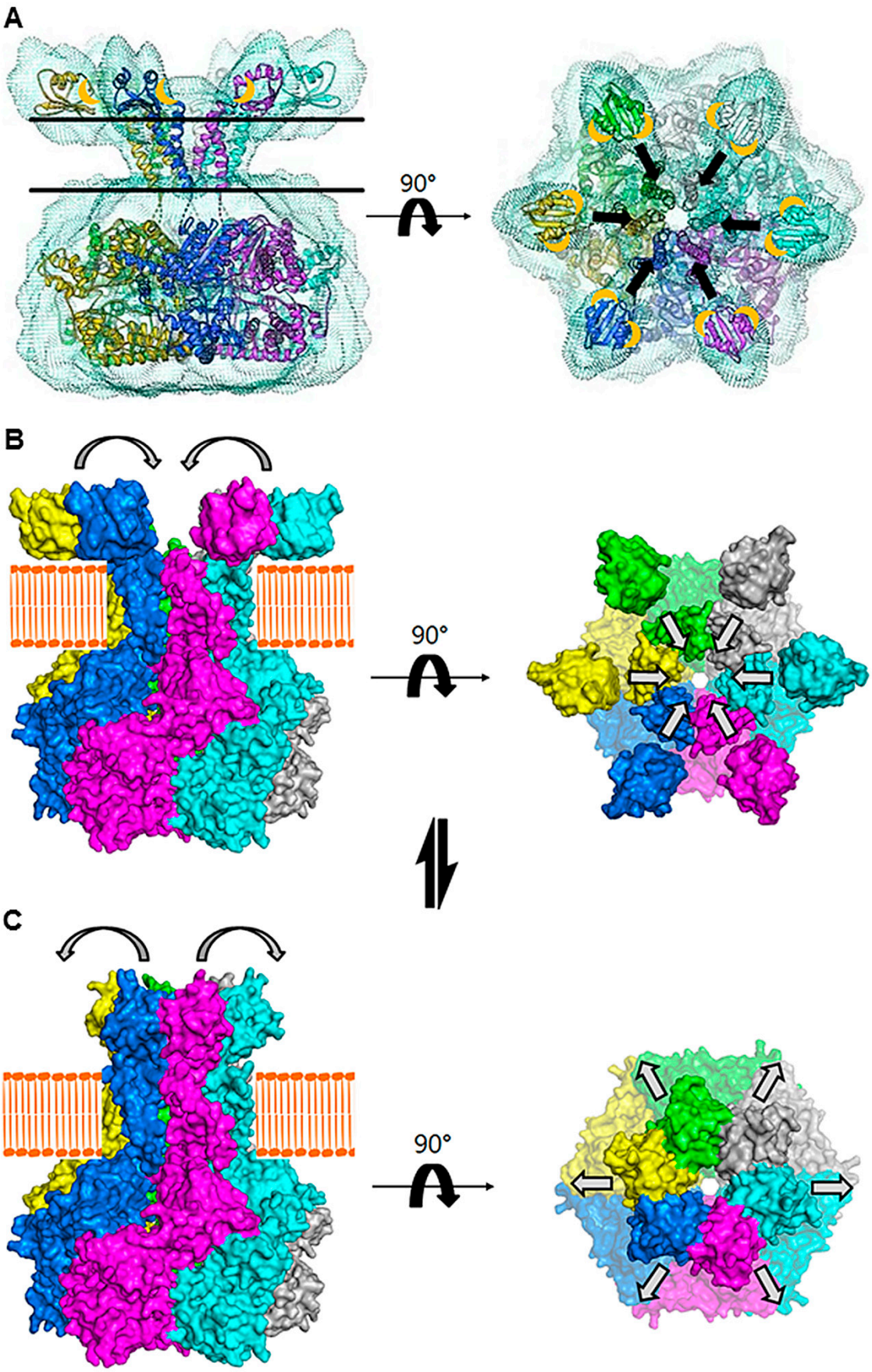

Preprints (www.preprints.org) | NOT PEER-REVIEWED | Posted: 29 December 2016 doi:10.20944/preprints201612.0145.v1

Figure 4. Model of FtsH dynamic structures. (A) Fitting of the *tm*FtsH structure onto the cryo-EM map of yeast mitochondrial AAA-protease (EMDB code EMD-1712). To build a *tm*FtsH structure, the PD (PDB code 4M8A), the TM obtained using Rosetta-Membrane, and the ATPase/protease domain (4EIW, 3KDS) were used. Hydrophobic patches are depicted in orange. (B) Model of the open-state structure in a lipid bilayer using monomeric *tm*PD. (C) Model of the closed-state structure in a lipid bilayer using hexameric *tm*PD.

3. Materials and methods

3.1. Cloning and site-directed mutagenesis

Coding DNA of *T. maritima* FtsH-PD (*tm*PD, residues 35-101) was amplified from cDNA by polymerase chain reaction (PCR) using a GeneAmp PCR system 2400 Thermocycler (Perkin Elmer, Waltham, USA). The forward (5'-GTCTACGGATCCAAGCTTAGCTACACGAG-3') and reverse (5'-CGTATTCTCGAGTTATCTCTCTCCCGAGAC-3') primers were designed using the MSB8 *tmFtsH* gene sequence in GenBank (Accession no. NC_000853; GeneID: 897649). The PCR product and a modified pET28a expression vector containing a tobacco etch virus (TEV) protease-cleavable (ENLYFQ/G) N-terminal His6-tag were digested using *Bam*HI and *Xho*I. The *tm*PD region of *FtsH* was ligated into the vector (pET28a/*tm*PD) and confirmed by sequencing. The *tm*PD mutant (D59N/D83N) was produced with PCR-based site-directed mutagenesis from the pET28a/*tm*PD plasmid using a GeneAmp PCR system 2400 Thermocycler (Perkin Elmer, Waltham,USA). The forward (5'-TGGGCCGTGAACAACTCGCAGCTCATA-3') and reverse (5'-CAGTACTCCGTCGTTCCTGATCACAAC-3') primers were designed to produce the desired amino acid substitutions.

3.2. Protein expression and purification

E. coli BL21 (DE3) cells were transformed with the pET28a/*tm*PD plasmid and grown overnight at 37°C in 50 mL of Luria Broth (LB) containing 50 μg/mL kanamycin. Cells were diluted in 3 L of LB, and grown at 37°C to an OD600 of 0.7. Protein expression was induced with 0.5 mM isopropyl-ß-D-thiogalactoside (IPTG). After inducing the cells for 8 h at 37°C, cells were harvested by low-speed centrifugation at 4°C. To label *tm*PD with seleno-L-methionine (SeMet), pET28a/*tm*PD was transformed into methionine-auxotrophic *E. coli* B834 (DE3) cells, which were inoculated into 1 L of LB containing 50 μg/mL kanamycin and grown at 37°C to an OD600 of 0.7. The cell pellet was washed three times in M9 minimal media without amino acids, and transferred into 2 L of M9 minimal media supplemented with 50 μg/mL SeMet, 0.4% (*w*/*v*) glucose, 2 mM magnesium sulfate, 0.1 mM calcium chloride, and 0.004% (*w*/*v*) thiamine and amino acids. Cells were grown at 37°C to an OD600 of 0.7, induced with 0.5 mM IPTG, and grown for an additional 24 h at 37°C. To purify native and SeMet-substituted *tm*PD, the cell pellet was resuspended in lysis buffer containing 50 mM sodium phosphate (pH 8.0), 5 mM imidazole, and 300 mM NaCl. Cells were lysed by sonication, and centrifuged at 14,000 *g* for 1 h. The supernatant was loaded onto a Bio-Rad gravity-flow column (Bio-Rad, Hercules, USA) packed with Ni-NTA agarose resin (Peptron, Daejeon, South Korea), which was pre-equilibrated in lysis buffer. The column was washed in buffer containing 50 mM sodium phosphate (pH 8.0), 30 mM imidazole, and 300 mM NaCl. The His-tagged protein was eluted in wash buffer containing 300 mM imidazole. The His6-tag was cleaved overnight at 4°C using TEV protease. Size exclusion chromatography was used to further purify *tm*PD using a HiLoad 16/60 Superdex-75 column (GE Healthcare Life Sciences, Marlborough, USA) pre-equilibrated in a buffer consisting of 20 mM Tris-HCl (pH 8.0) and 100 mM NaCl. The elution profile showed a peak corresponding to an 8 kDa protein, indicating that purified *tm*PD is a monomer. *tm*PD was pooled and concentrated to 19 mg/ml for the native protein, and 13.7 mg/ml for the SeMet-substituted protein using Centriprep 3 KD cutoff (Merck Millipore, Billerica, USA). Samples were stored at -80°C.

Preprints (www.preprints.org) | NOT PEER-REVIEWED | Posted: 29 December 2016 doi:10.20944/preprints201612.0145.v1

3.3. Crystallization, structure determination, and modeling

The hanging-drop vapor diffusion method was used to crystallize *tm*PD. For the native protein, 1 μl of protein was mixed with 1 μl of reservoir solution containing 25% (*w*/*v*) PEG 3350, 0.1 M sodium citrate (pH 5.5), and 0.2 M lithium sulfate. For the SeMet-incorporated protein, 1 μl of reservoir solution containing 15% (*w*/*v*) PEG 2000 and 0.1 M MES-NaOH (pH 6.0) was used. Native data were collected at a 1.50 Å resolution and SeMet multiwavelength anomalous dispersion (MAD) data were collected at a 1.95 Å resolution at the Pohang Accelerator Laboratory (Pohang, Korea). Data were processed using HKL2000 [28] and summarized in Table 1. The SeMet MAD structure was determined using SOLVE/RESOLVE [29,30], and the isomorphous native structure was solved using difference Fourier methods with the SeMet model. Initial models were built and rebuilt using Coot and refined using PHENIX [31,32], as summarized in Table 1.

For the generation of the PD hexamer model, we applied a 2-fold operation along a pseudo 6-fold axis using a trimer in an asymmetric unit that was related by a pseudo 6-fold symmetry.

3.4. Hydrodynamic radius measurement of pH-dependent PD oligomerization

The hydrodynamic radius (R_H) of *tm*PD was measured using the dynamic light scattering method (Avidnano W130i and the *i*-Size™ software, High Wycombe, UK). Briefly, 18 mg/mL of *tm*PD was added to a solution containing 100 mM NaCl and 100 mM buffer (sodium citrate for pH 4.5-5.5, MES-NaOH for pH 5.6-6.5, HEPES-NaOH for pH 7.0-7.5, and Tris-HCl for pH 8.0-8.5). Three measurements were used to calculate the average R_H and standard deviation at each pH at 20°C. The curve R_H as a function of pH was fitted using the formulas (Wild type, $R_H = 9.7279e^{-0.234pH}$; D59N/D83N Mutant, $R_H = 8.3626e^{-0.182pH}$). Theoretical R_H values for monomeric, dimeric, trimeric, and hexameric *tm*PD were calculated using Hydropro [20].

Acknowledgments: We thank the staff at beamline BL-5C (PAL-4A) of the Pohang Accelerator Laboratory (Pohang, South Korea), beamline 5A at the Photon Factory (Tsukuba, Japan), and beamline BL26B1 at Spring-8 (Harima, Japan) for their kind help with data collection and thank Professor E. M. Engelman for discussion and suggestions during the course of this study. This work was supported by grants from the National Research Foundation (NRF) of the Republic of Korea (Grant numbers: 2013M3A9A7046297, 2013R1A2A2A01068440, and 2015M2A2A4A03044653). Founding agencies had no role in the study design, data analysis, or publication of results.

Author contributions: Jimin Wang and Soo Hyun Eom designed the research; Jun Yop An, Kyung Jin Park, Humayun Sharif, Gil Bu Kang conducted purification and crystallization; Jun Yop An, Jung-Gyu Lee collected the X-ray data; Jun Yop An, Humayun Sharif, Gil Bu Kang solved the structure; Sukyeong Lee, Mi Sun Jin, and Ji-Joon Song analyzed the data. Jun Yop An, Jimin Wang, and Soo Hyun Eom wrote the manuscript. All authors read and agreed with the final manuscript.

Conflicts of interest: The authors declare no conflict of interest.

 doi:10.20944/preprints201612.0145.v1

References

1. Janska, H.; Kwasniak, M.; Szczepanowska, J. Protein quality control in organelles-AAA/FtsH story. *Biochim. Biophys. Acta* **2013**, 1833, 381-387.

2. Ito, K.; Akiyama, Y. Cellular functions, mechanism of action, and regulation of FtsH Protease. *Annu. Rev. Microbiol.* **2005**, 59, 211-231.

3. Leonhard, K.; Stiegler, A.; Neupert, W.; Langer, T. Chaperone-like activity of the AAA domain of the yeast Yme1 AAA protease. *Nature* **1999**, 398, 348-351.

4. Bieniossek, C.; Thomas, S.; Mario, B.; Markus, M.; Reto, M.; Ulrich, B. The molecular architecture of the metalloprotease FtsH. *Proc. Natl. Acad. Sci. USA* **2006**, 103, 3066-3071.

5. Yamamoto, Y.; Aminaka, R.; Yoshioka, M.; Khatoon, M.; Komayama, K.; Takenaka, D.; Yamashita, A.; Nijo, N.; Inagawa, K.; Morita, N.; Sasaki, T.; Yamamoto, Y. Quality control of photosystem II: impact of light and heat stresses. *Photosynth. Res.* **2008**, 98, 589-608.

6. Cheregi, O.; Sicora, C.; Kós, P.B.; Barker, M.; Nixon, P.J.; Vass, I. The role of the FtsH and Deg proteases in the repair of UV-B radiation-damaged Photosystem II in the cyanobacterium Synechocystis PCC 6803. *Biochim. Biophys. Acta* **2007**, 1767, 820-828.

7. Tomoyasu, T.; Yamanaka, K.; Murata, K.; Suzaki, T.; Bouloc, P.; Kato, A.; Niki, H.; Hiraga, S.; Ogura, T. Topology and subcellular localization of FtsH protein in Escherichia coli. *J. bacteriol*. **1993**, 175, 1352-1357.

8. Akiyama, Y.; Ito, K. Roles of homooligomerization and membrane association in ATPase and proteolytic activities of FtsH in vitro. *Biochemistry* **2001**, 40, 7687-7693.

9. Saikawa, N.; Akiyama, Y.; Ito, K. FtsH exists as an exceptionally large complex containing HflKC in the plasma membrane of Escherichia coli. *J. Struct. Biol.* **2004**, 146, 123-129.

10. Akiyama, Y. Proton-motive force stimulates the proteolytic activity of FtsH, a membrane-bound ATP-dependent protease in Escherichia coli. *Proc. Natl. Acad. Sci. USA* **2002**, 99, 8066-8071.

11. Westphal, K.; Langklotz, S.; Thomanek, N.; Narberhaus, F. A trapping approach reveals novel substrates and physiological functions of the essential protease FtsH in Escherichia coli. *J. Biol. Chem*. **2012**, 283, 42962-42971.

12. Arends, J.; Thomanek, N.; Kuhlmann, K.; Marcus, K.; Narberhaus, F. In vivo trapping of FtsH substrates by label-free quantitative proteomics. *Proteomics* **2016**, 16, 3161-3172.

13. Hari, S.B.; Sauer, R.T. The AAA+ FtsH Protease Degrades an ssrA-Tagged Model Protein in the Inner Membrane of Escherichia coli. *Biochemistry* **2016**, 40, 5649-5652.

14. Taura, T.; Baba, T.; Akiyama, Y.; Ito, K. Determinants of the quantity of the stable SecY complex in the Escherichia coli cell. *J. Bacteriol*. **1993**, 175, 7771-7775.

15. von Heijne, G. Introduction to theme "membrane protein folding and insertion". *Ann. Rev. Biochem.* **2011**, 80, 157-160.

16. Sauer, R.T.; Baker, T.A. AAA+ proteases: ATP-fueled machines of protein destruction. *Ann. Rev. Biochem.* **2011**, 80, 587-612.

17. Okuno, T.; Yamanaka, K.; Ogura, T. An AAA protease FtsH can initiate proteolysis from internal sites of a model substrate, apo-flavodoxin. *Genes Cells* **2006**, 11, 261-268.

18. Wilks, J.C.; Slonczewski, J. L. pH of the cytoplasm and periplasm of Escherichia coli: rapid measurement by green fluorescent protein fluorimetry. *J. Bacteriol.* **2007**, 189, 5601-5607.

19. von Heijne, G. Membrane protein structure prediction. Hydrophobicity analysis and the positive-inside rule. *J. Mol. Biol.* **1992**, 225, 487-494.

20. García de la Torre, J.; Huertas, M.L.; Carrasco, B. Calculation of hydrodynamic properties of globular proteins from their atomic-level structure. *Biophys. J.* **2000**, 78, 719-730.

21. Scharfenberg, F.; Serek-Heuberger, J.; Coles, M.; Hartmann, M.D.; Habeck1, M.; Martin, J.; Lupas, A.N.; Alva, V. Structure and evolution of N-domains in AAA. *J. Mol. Biol.* **2015**, 427, 910-923

22. Jeanmougin, F.; Thompson, J.D.; Gouy, M.; Higgins, D.G.; Gibson, T.J. Multiple sequence alignment with Clustal X. *Trends Biochem. Sci.* **1998**, 23, 403-405.

23. Robert, X.; Gouet, P. Deciphering key features in protein structures with the new ENDscript server. *Nucleic Acids Res.* **2014**, 42, 320-324.

24. Korbel, D.; Wurth, S.; Käser, M.; Langer, T. Membrane protein turnover by the m-AAA protease in mitochondria depends on the transmembrane domains of its subunits. *EMBO Rep.* **2004**, 5, 698-703.

25. Ramelot, T.A.; Yang, Y.; Sahu, I.D.; Lee, H.; Xiao, R.; Lorigan, G.A.; Montelione, G.T.; Kennedy, M.A. NMR structure and MD simulations of the AAA protease intermembrane space domain indicates peripheral membrane localization within the hexaoligomer. *FEBS Lett.* **2013**, 587, 3522-3528.

26. Lee, S.; Augustin, S.; Tatsuta, T.; Gerdes, F.; Langer, T.; Tsai, F.T. Electron cryomicroscopy structure of a membrane-anchored mitochondrial AAA protease. *J. Biol. Chem.* **2011**, 286, 4404-4411.

27. Vinyard, D.J.; Ananyev, G.M.; Dismukes, G.C. Photosystem II: the reaction center of oxygenic photosynthesis. *Annu. Rev. Biochem.***2013**, 82, 577-606.

28. Otwinowski, Z.; Minor, W. Processing of X-ray diffraction data collected in oscillation mode. *Methods Enzymol.* **1997**, 276, 307-326.

29. Terwilliger, T.C.; Berendzen, J. Automated MAD and MIR structure solution. *Acta Crystallogr. D* **1999**, 55, 849-861.

30. Terwilliger, T.C. Maximum-likelihood density modification. *Acta Crystallogr. D* **2000**, 56, 965-972.

31. Emsley, P.; Cowtan, K. Coot: model-building tools for molecular graphics. *Acta Crystallogr. D* **2004**, 60, 2126-2132.

32. Adams, P.D.; Afonine, P.V.; Bunkóczi, G.; Chen, V.B.; Davis, I.W.; Echols, N.; Headd, J.J.; Hung, L.; Kapral, G.J.; Grosse-Kunstleve, R.W.; McCoy, A.J.; Moriarty, N.W.; Oeffner, R.; Read, R.J.; Richardson,

D.C.; Richardson, J.S.; Terwilliger, T.C.; Zwart, P.H. PHENIX: a comprehensive Python-based system for macromolecular structure solution. *Acta Crystallogr. D* **2010**, 66, 213-221.